molbank

MDPI

Communication

A Simple and Efficient Approach to the Synthesis of 4-Aryl-2-dialkylphosphonomethyl-4-oxobutanenitrile

Ferid Yaccoubi [1,2], Hitham Elleuch [1], Hussein S. Mohamed [3,4], Zeinab S. Hamza [3] and Yasser H. Zaki [2,5,*]

[1] Laboratoire de Chimie Organique Structurale LR99ES14, Faculté des Sciences de Tunis, Université de Tunis El Manar, Campus Universitaire, Tunis 2092, Tunisia; feridyacc@su.edu.sa (F.Y.); yzaki1973@gmail.com (H.E.)
[2] Department of Chemistry, Faculty of Science and Humanity Studies at Al Quwayiyah, Shaqra University, Al-Quwayiyah 19245, Saudi Arabia
[3] Chemistry of Natural Products, Research Institute of Medicinal and Aromatic Plants (RIMAP), Beni-Suef University, Beni-Suef 62514, Egypt; h_gendy_2010@yahoo.com (H.S.M.); alaa2562003@gmail.com (Z.S.H.)
[4] Basic Sciences Department, Higher Technological Institute, Beni-Suef 62514, Egypt
[5] Department of Chemistry, Faculty of Science, Beni-Suef University, Beni-Suef 62514, Egypt
* Correspondence: yzaki2002@yahoo.com; Tel.: +966-564140012

Abstract: In this work, we describe a simple and easy synthetic approach to variously 4-aryl-2-alkylphosphonomethyl-4-oxobutanenitrile based on the reaction of aromatic aldehydes with phosphorylated Michael's acceptors in good yields. A general mechanism for the reactions was also proposed. Characterization of the products was carried out by several spectroscopic tools, including Infrared and Nuclear Magnetic Resonance Spectroscopies (^{1}H, ^{13}C, and ^{31}P-NMR). Molecular docking studies were conducted on the synthesized materials against (1UK4) the crystal structure of the SARS Coronavirus Main Proteinase (3CLpro) to study the antiviral activity of these compounds and against (1E3K) the Human Progesterone Receptor to study the anticancer activity of these compounds. We found that compound (**5i**) was the best one in both antiviral and anticancer activity (according to the binding energy values).

Keywords: benzaldehyde; 2-dialkylphosphonomethylpropenenitrile; 4-aryl-2-alkylphosphonomethyl-4-oxobutanenitrile; molecular docking antiviral

Citation: Yaccoubi, F.; Elleuch, H.; Mohamed, H.S.; Hamza, Z.S.; Zaki, Y.H. A Simple and Efficient Approach to the Synthesis of 4-Aryl-2-dialkylphosphonomethyl-4-oxobutanenitrile. *Molbank* **2022**, *2022*, M1342. https://doi.org/10.3390/M1342

Academic Editor: Ian R. Baxendale

Received: 30 December 2021
Accepted: 2 February 2022
Published: 15 February 2022

1. Introduction

For a long time, compounds with both a carbonyl and a nitrile function piqued the interest of several researchers due to their potential utility as reagents in organic synthesis [1]. Many of these compounds have several biological activities [2], and numerous methods of synthesis are described in the literature [3,4]. The starting substrate used is most often acrylonitrile.

To our knowledge, 4-aryl-2-alkylphosphonomethyl-4-oxobutanenitrile is not described in the literature. We were inspired by these works, particularly those of Stetter and others [5,6]. At the start of this year, the world was shocked when severe acute respiratory syndrome (SARS) was discovered in the Chinese province of Hubei and spread rapidly. There are more than 200 districts in China nowadays. Around the world, there are a variety of countries and territories [7]. The genome shares a lot of similarities with the SARS-Cove genome. The outbreak began in early 2003 and lasted into the summer of that year [8]. The majority of the Coronaviridae genome encodes two polypeptides [9] pp1a and pp1ab, which are translated via ribosomal frame shifting. The two proteases, 3CLpro (3C-like protease) and 3Cpro (3C protease), break these polypeptides and turn them into mature nonstructural proteins (NSPs). The open reading frame 1 encodes PLpro (Papain Like Protease) [10]. The structure of 3CLpro from SARS-CoV-2 (PDB code 6LU7) differs from

the accessible structure of 3CLpro from SARS-CoV-2 (PDB code 1UK4) by just 12 amino acids [11], with carbon atoms all situated at least 1 nm away from the 3CLpro active site, according to the latest research [12].

Breast cancer is one of the leading causes of death worldwide, including in Indonesia. according to a 2008 data study, 1/3 of women per 1000 people were diagnosed with breast cancer [13]. According to the Indonesian Ministry of Health's data and information Centre, there were 819 new breast cancer cases in 2013, with 217 deaths. Every year, the number continues to rise [14]. In KEGG, the breast cancer pathway is shown. It demonstrates that the progesterone receptor (PR) is the most effective route [15]. Publicity is an important aspect of every business. In breast cancer, it plays a vital role in cell proliferation. The natural public relations ligand is progesterone. When progesterone attaches to PR, it causes cell proliferation, which promotes cancer cell growth. The suppression of PR by drugs known as Selective Progesterone Receptor Modulators (SPRMs), which compete with the hormone progesterone, prevents cancer cells from proliferating [16]. In continuation of our recent work aimed at the synthesis of biologically active compounds [17–21], we intend to synthesize a series of 4-aryl-2-phosphonomethyl-4-oxobutanenitriles using the aromatic aldehyde and 2-dialkylphosphonomethylpropenenitriles in this work.

2. Results and Discussion

Chemistry

In recent studies carried out in our laboratory, we showed that dialkylphosphonomethyl-propenenitriles **3**, obtained from the Arbuzov reaction with Mannich base [12,22], (Scheme 1) behave as bilectrophilic agents [23,24]. Their double bond, strongly activated by the presence of the nitrile function and the phosphono group, easily adds nucleophiles [25].

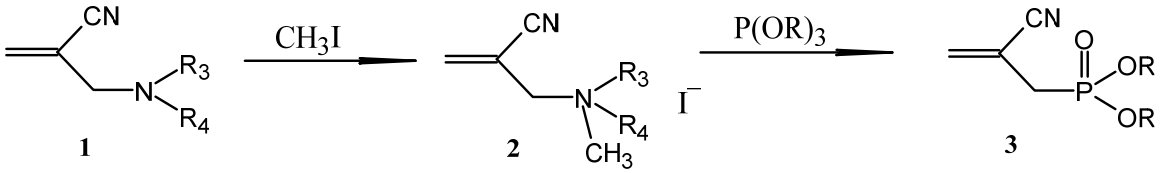

Scheme 1. Synthesis of 2-dialkylphosphonomethylpropenenitrile **3**.

The condensation of one equivalent of the aromatic aldehyde and one equivalent of 2-dialkylaminomethyl-propenenitrile **3** in DMF in the presence of a catalytic amount of 3-ethyl-5-(2-hydroxyethyl)-4-methylthiazolium bromide and triethylamine leads to product **5** in a good yield, and the product obtained is 4-aryl-2-dialkylaminomethyl-4-oxobutanenitrile (Scheme 2). The structure of isolable products was characterized by spectral (IR, ^{1}H-NMR, MS) and elemental analysis data (see experimental). (Figures S9–S26). The IR spectra produced on some 4-aryl-2-methylamino-4-oxobutanenitrile **5** have a nitrile band at around 2247 cm^{-1}, characteristic of the CN group, and a band around 1685 cm^{-1}, characteristic of the carbonyl group. The absence of the absorption band of the nitrile bond on the IR spectra allowed us to follow the evolution of the formation reaction of the product **5**. The analysis of proton and ^{13}C-NMR spectra confirms the proposed structures. The addition of aldehyde to the double bond of alkylphosphonopropenenitriles **3** results in ^{1}H-NMR by the disappearance of the ethylene protons to 5.5–6.0 ppm and the appearance of a signal at 3.2 ppm attributable to the protons of the CH_2-CO motif. Examination of the ^{13}C-NMR spectra of 4-aryl-2-methylamino-4-oxobutanenitrile **5** shows the disappearance of signals of the two ethylenic carbons of 2-phosphonomethylpropenenitrile, which resonate at 118 and 121 ppm, and the appearance of a signal at about 198 ppm relative to the carbon of the C=O unit. The ^{1}H, ^{13}C, and ^{31}P-NMR attributions of the 4-aryl-2-methylamino-4-oxobutanenitrile compounds were carried out by referring to the bibliographic data. The proton, ^{31}P, and ^{13}C-NMR data of the compounds **5** are recorded in the experimental part.

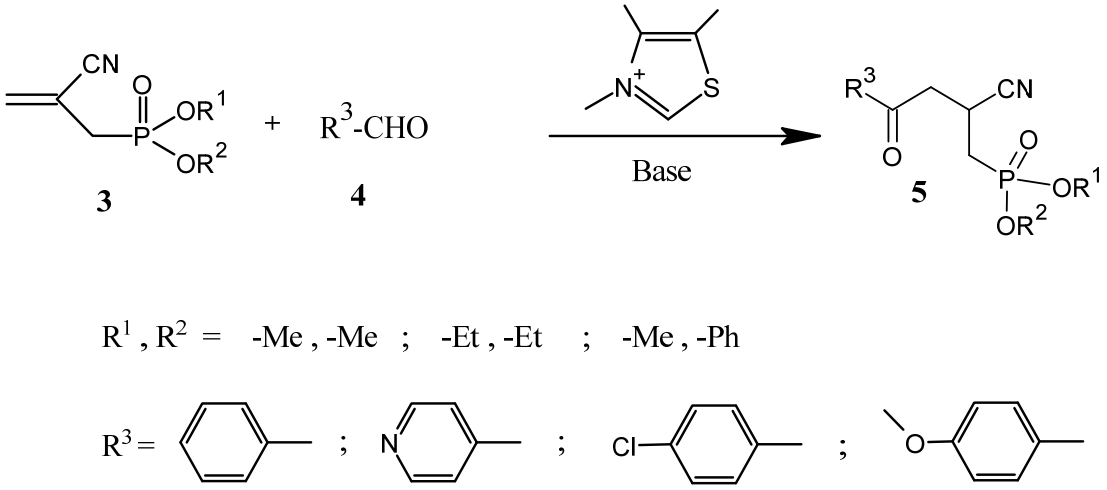

Scheme 2. Synthesis of 4-aryl-2-dialkylphosphonomethyl-4-oxobutanenitrile **5**.

The first step of this reaction mechanism (Scheme 3) goes through the formation of catalyst **II** by deprotonation of the precatalyst, the thiazolium salt **I**. This mechanism is identical to that which was proposed by Breslow for the benzoin reaction [26].

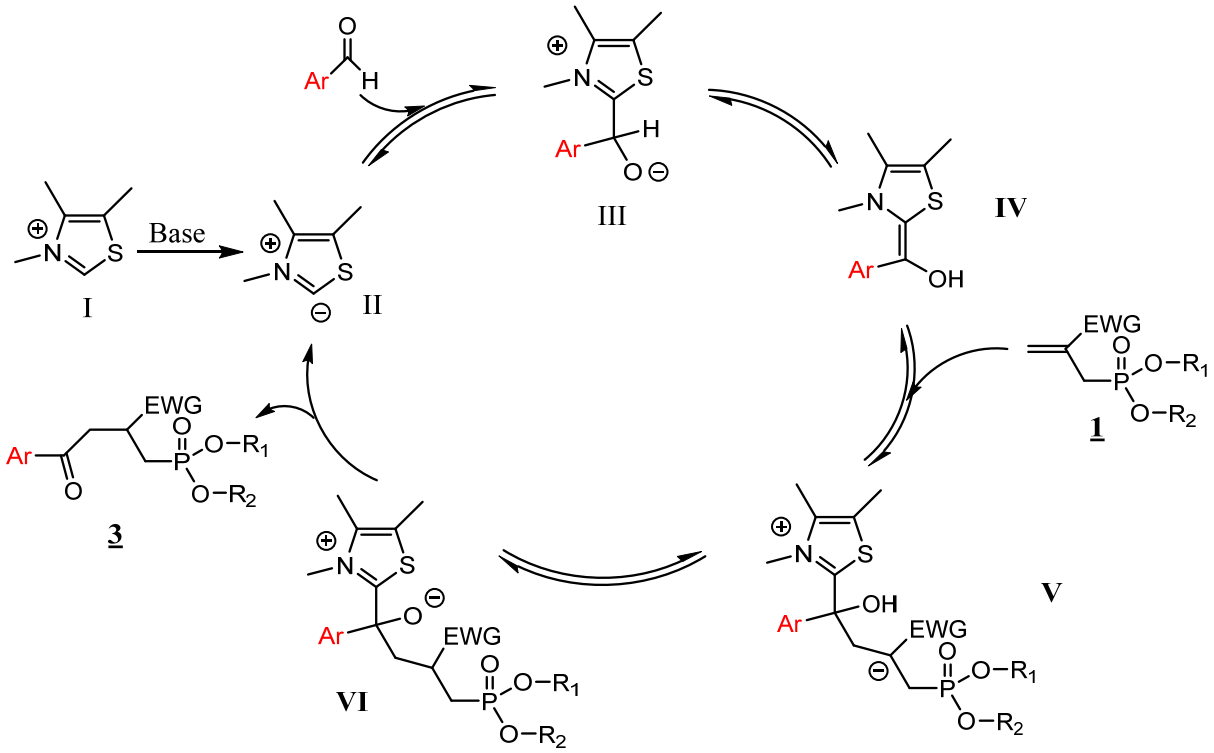

Scheme 3. A general mechanism for the reactions.

Once the catalyst is formed, it can be added to the aldehyde to form the intermediary **III**, which, by proton exchange, will generate the compound **IV**, known as the Breslow intermediate. This is the last one who will be able to add 1.4 to Michael's acceptor to form the new intermediate **V**, which, after proton exchange, forms compound **VI**. The removal of catalyst **II** releases the product of the Stetter reaction **5**, and a new catalytic cycle begins. There may be some competition between the additions of 1, 2 and 1, 4 of the Breslow intermediate **IV**. Indeed, it can be added to Michael's acceptor to generate product **V**, or react with a second equivalent of aldehyde to give the product benzoin. However, the

formation of the product benzoin is reversible, which ultimately favors the formation of product **V**.

3. Molecular Docking Study

For each synthesized compound, the docking simulation process was completed, and the best conformation was chosen as the compound with the highest negative binding energy value. Figures S1–S4 illustrate the 2D and 3D structures of the ligand–receptor interactions of the synthesized compounds with (1UK4). Figures S5–S8 illustrate the 2D and 3D structures of the ligand–receptor interactions of the synthesized compounds with (1E3K). Table 1 displays the estimated binding energies produced by docking the synthesized materials with 1UK4 and 1E3K. All the compounds studied formed stable complexes with receptors that had a high binding energy. According to our findings, compound **5i** had the best docking energy (highest binding energy), with a binding affinity of −8.65 kcal/mol with 1UK4 and −10.41 kcal/mol with 1E3K). As a result, the compounds studied, particularly compound **5i**, have the potential to be used in antiviral and anticancer applications. According to molecular docking, the most interacting residues of 1UK4 in the **5i** compound active site were HIS 161, CYS 143, SER 142, and MET 47. But in 1E3K, it interacted with CYS 209, TYR 208, PHE 96, MET 77, GLN 43, LEU 39, and LEU 38.

Table 1. Binding energies produced from molecular docking for all studied compound with (**1uk4**) and (**1e3k**).

Compounds	(1uk4) Binding Energy (ΔG)kcal/mol	(1e3k) Binding Energy (ΔG)kcal/mol
3a	−6.34	−6.64
3b	−6.67	−6.94
3e	−7.01	−9.01
5a	−8.20	−9.08
5b	−7.32	−9.39
5c	−7.91	−9.67
5d	−7.99	−8.01
5e	−8.44	−8.56
5f	−9.14	−9.09
5g	−7.01	−8.05
5h	−6.46	−9.56
5i	−8.65	−10.41
5j	−7.36	−8.77
5k	−6.83	−9.49

4. Material and Methods

4.1. Chemistry

Solvents and reagents were obtained from commercial sources and were dried and purified when necessary using standard techniques. IR spectra of the compound **5** derivatives were made in chloroform on a Perkin–Elmer Paragon 1000 PC spectrometer. The wave numbers were expressed in cm^{-1}. The ^{1}H, ^{31}P, and ^{13}C-NMR spectra were recorded in solution in $CDCl_3$ on a Brucker AC 300 using TMS and H_3PO_4 as an internal reference. The chemical shifts were expressed in ppm. The multiplicity of signals was indicated by the following abbreviations: s: singlet, d: doublet, t: triplet, m: multiplet, md: doubled multiplet. Coupling constants were reported in Hertz (Hz). Purification of the products was carried out by chromatography on silica gel using a mixture of ether and petroleum ether as eluent, the proportion of which was 20/80. Chromatography on a thin layer of silica gel 0.2 mm thick with a fluorescent indicator at 254 nm using ether and petroleum ether in a 20/80 ratio as eluent was used to monitor the progress of the reaction.

4.2. General Procedure for the Preparation of 2-Dialkylphosphonomethylpropenenitrile **3**

4.2.1. Step 1: Preparation of the Ammonium Salt

A 20 mL methanol solution of 3-(morpholinomethyl) propene nitrile (3 g, 15 mmol) was treated with 2.84 g (20 mmol) methyl iodide. The reaction mixture was maintained for 4 h with stirring at 40 °C. After cooling, the solvent was evaporated under a vacuum. The resulting quaternary ammonium salt was used in its crude state.

4.2.2. Step 2: Synthesis of Allylphosphonates **3**

To the quaternary ammonium obtained previously, 20 mmol of alkoxyphosphite and 20 mL of anhydrous benzene were added. The mixture was heated under reflux for two hours. After cooling, the residual ammonium salt was filtered off, the benzene was evaporated off, and the product obtained was either distilled under reduced pressure or purified by column chromatography using ethyl acetate as an eluent.

Dimethyl (2-cyanoallyl)phosphonate **3a**. $Eb_{0,1}$ = 92 °C. Rdt = 82%. IR: $\nu_{P=O}$ = 1263 cm^{-1}; $\nu_{C=C}$ = 1631 cm^{-1}; ν_{CN} = 2246 cm^{-1}. ^{31}P-NMR: δ = 25.4. ^{1}H-NMR: δ = 3.43 (d, 2H, $^{2}J_{PH}$ = 22 Hz, -CH_2-P), 3.70 (d, 6H, $^{3}J_{HH}$ = 7.9 Hz, CH_3-O-), 5.78 (d, 1H, $^{4}J_{PH}$ = 5.1 Hz), 6.26 (d, 1H, $^{4}J_{PH}$ = 5.5 Hz). ^{13}C-NMR (75 MHz, $CDCl_3$): δ: C_1: 135.4; C_2: 118.0 ($^{2}J_{P-C}$ = 7.5 Hz); C_3: 119.4; C_4: 35.2 ($^{1}J_{P-C}$ = 133 Hz), C5: 52.9 ($^{2}J_{P-C}$ = 6.4 Hz). Combustion elemental analysis calculated for $C_6H_{10}NO_3P$ (175.04): C, 41.15; H, 5.76; N, 8.00. Found C, 41.25; H, 5.84; N, 8.11%.

Diethyl (2-cyanoallyl)phosphonate **3b**. $Eb_{0,4}$ = 103 °C. Rdt = 86%. IR: $\nu_{P=O}$ = 1260 cm^{-1}; $\nu_{C=C}$ = 1630 cm^{-1}, ν_{CN} = 2252 cm^{-1}. ^{31}P-NMR: δ = 25.2. ^{1}H-NMR: δ = 1.30 (t, 6H; $^{3}J_{H-H}$ = 7.5 H, CH_3-), 3.45 (d, 2H, $^{2}J_{PH}$ = 18 Hz, -CH_2-P), 4.23 (m, 4H, -O-CH_2-), 5.63 (d, $^{4}J_{PH}$ = 5.1 Hz, 1H), 6.12 (d, $^{4}J_{PH}$ = 5.4 Hz, 1H). ^{13}C-NMR (75 MHz, $CDCl_3$): δ: C_1: 135.6; C_2: 117.6; C_3: 119.5; C_4: 34.2 ($^{1}J_{P-C}$ = 133 Hz), C_5: 62.8 ($^{2}J_{P-C}$ = 6.5 Hz); C_6: 16.3. Combustion elemental analysis calculated for $C_8H_{14}NO_3P$ (203.07): C, 47.29; H, 6.95; N, 6.89. Found C, 47.35; H, 7.04; N, 6.98%.

Methyl phenyl (2-cyanoallyl)phosphonate **3c**. $Eb_{0,4}$ = 115 °C. Rdt = 85%. IR: $\nu_{P=O}$ = 1255 cm^{-1}; $\nu_{C=C}$ = 1628 cm^{-1}; ν_{CN} = 2252 cm^{-1}. ^{31}P-NMR: δ = 42.7. ^{1}H-NMR: δ = 3.65 (d, 2H, $^{2}J_{PH}$ = 18 Hz, -CH_2-P), 3.70 (d, 3H, $^{3}J_{P-H}$ = 10.5 Hz, -O-CH_3), 5.74 (d, $^{4}J_{P-H}$ = 5.1 Hz, 1H), 6.29 (d, $^{4}J_{P-H}$ = 5.4 Hz, 1H), 7.48–7.79 (m, 5H, Ph). ^{13}C-NMR (75 MHz, $CDCl_3$): δ: C_1: 136.5; C_2: 117.9; C_3: 119.5; C_4: 35.7 ($^{1}J_{P-C}$ = 133 Hz), C_5: 53.7 ($^{2}J_{P-C}$ = 8 Hz); C_6: 130.6. C_7: 131.4. C_8: 128.0. C_9: 132.2. Combustion elemental analysis calculated for $C_{11}H_{12}NO_3P$ (237.06): C, 55.70; H, 5.10; N, 5.91. Found C, 55.79; H, 5.18; N, 6.00%.

4.3. General Procedure for the Preparation of 4-Aryl-2-dialkylphosphonomethyl-4-oxobutanenitrile **5**

We describe, for example, the preparation of compound **5a**. In a 500 mL three-necked flask equipped with a refrigerant fitted with a drying tube and a dropping funnel mounted with a tube of nitrogen, a solution of 3-ethyl-5-(2-hydroxyethyl)-4-methylthiazolium bromide 2.52 g (0.01 mol) in 150 mL of dry *N*,*N*-dimethylformamide was introduced after thorough purging with dry nitrogen. The flask was immersed in a water bath maintained at 60 °C and 6.06 g of triethylamine (0.06mol) was added rapidly from the dropping funnel. After 30 min of agitation, 10.6 g of benzaldehyde (0.1mol) was added dropwise to this solution over a period of 30 min. After stirring for one hour, 2-dialkylaminopropenenitrile (**3a**), freshly distilled at 17.5 g (0.1 mol), was added over a period of one hour. The solution became more and more viscous. After 12 h of stirring, 30 mL of acetic acid (1 M) was added and stirring continued for another 5 min. The solvent was removed with a rotary evaporator, and the residue was dissolved in 100 mL of water. The solution was extracted several times with chloroform (4 × 100 mL). After drying with anhydrous magnesium sulfate, the solvent was evaporated under reduced pressure and the residual liquid was purified on a column of silica gel (ether, petroleum ether 20/80).

Dimethyl (2-cyano-4-oxo-4-phenylbutyl)phosphonate **5a** (Figure 1). Yield = 79%; viscous. IR: $\nu_{P=O}$ = 1249 cm^{-1}; $\nu_{C=O}$ = 1683 cm^{-1}; ν_{CN} = 2251 cm^{-1}. ^{31}P-NMR: δ = 31.87. ^{1}H-NMR: (300 MHz, $CDCl_3$) δ: 2.41 ppm (2H, md, J_{P-H} = 19.6 Hz, -CH_2-P); 3.24 ppm (2H, m, -CH_2-C=O); 3.71 ppm (6H, d, $^{3}J_{P-H}$ = 10.2 Hz, -O-CH_3); 3.77 ppm (1H, m, >CH-); 7.49–7.95 ppm (5H, m, Ph). ^{13}C-NMR (300 MHz, $CDCl_3$) δ: C_1: 198.1; C_2: 39.6 (J_{P-C} = 9.6 Hz); C_3: 29.1 (J_{P-C} = 10.3 Hz); C_4: 122.4 (J_{P-C} = 5.1 Hz); C_5: 29.0 (J_{P-C} = 133 Hz); C_6: 52.9 (J_{P-C} = 6.3 Hz); C_7: 136.6; C_8: 128.40; C_9: 128.93; C_{10}: 133.42. Combustion elemental analysis calculated for $C_{13}H_{16}NO_4P$ (281.08): C, 55.52; H, 5.73; N, 4.98. Found C, 55.66; H, 5.86; N, 5.08%.

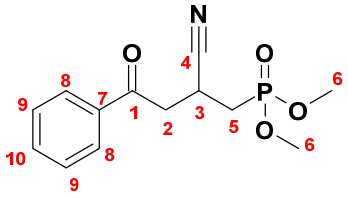

Figure 1. The structure of compound **5a**.

Diethyl (2-cyano-4-oxo-4-phenylbutyl)phosphonate **5b** (Figure 2). Yield = 76%; viscous. IR: $\nu_{P=O}$ = 1253 cm^{-1}; $\nu_{C=O}$ = 1685 cm^{-1}; ν_{CN} = 2247 cm^{-1}. ^{31}P-NMR: δ = 30.90. ^{1}H-NMR: δ: 1.35 ppm (6H, t, $^{3}J_{H-H}$ = 7.5 Hz, -CH_3); 2.46 ppm (2H, md, $^{2}J_{P-H}$ = 22 Hz, -CH_2-P); 3.26 ppm (2H, m, -CH_2-C = O); 3.77 ppm (1H, m, >CH-); 4.10 ppm (4H, m, -CH_2-O); 7.51–7.91 ppm (5H, m, Ph). ^{13}C-NMR (300 MHz, $CDCl_3$) δ: C_1: 198.2; C_2: 39.8 (J_{P-C} = 9.7 Hz); C_3: 28.7 (J_{P-C} = 10.1 Hz); C_4: 121.9 (J_{P-C} = 5.1 Hz); C_5: 28.7 (J_{P-C} = 138 Hz); C_6: 61.7 (J_{P-C} = 6.5 Hz); C_7: 137.2; C_8: 128.40; C_9: 128.96; C_{10}: 133.61; C_{11}: 16.35. Combustion elemental analysis calculated for $C_{15}H_{20}NO_4P$ (309.11): C, 58.25; H, 6.52; N, 4.53. Found C, 58.33; H, 6.61; N, 4.63%.

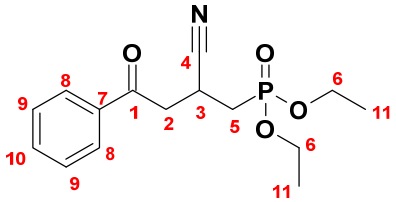

Figure 2. The structure of compound **5b**.

Methyl phenyl (2-cyano-4-oxo-4-phenylbutyl)phosphonate **5c** (Figure 3). Yield = 75%; viscous. IR: $\nu_{P=O}$ = 1257 cm^{-1}; $\nu_{C=O}$ = 1679 cm^{-1}; $\nu_{C\,N}$ = 2253 cm^{-1}. ^{31}P-NMR: δ = 39.91. ^{1}H-NMR: δ: 2.71 ppm (1H, m, -CH_2-P); 2.98 ppm (1H, m, -CH_2-P); 3.25 ppm (2H, m, -CH_2-C=O); 3.71 ppm (3H, d, $^{3}J_{P-H}$ = 10.5 Hz, CH_3-O); 3.82 ppm (1H, m, >CH-); 7.50–7.90 ppm (10H, m, Ph). ^{13}C-NMR (300 MHz, $CDCl_3$) δ: C_1: 197.7; C_2: 39.9 (J_{P-C} = 8.9 Hz); C_3: 29.2 (J_{P-C} = 8.7 Hz); C_4: 122.2 (J_{P-C} = 4.2 Hz); C_5: 30.5 (J_{P-C} = 96.7 Hz); C_6: 53.3 (J_{P-C} = 6.8 Hz); C_7: 137.1; C_8: 128.45; C_9: 128.65; C_{10}: 132.90; C_{11}: 132.12 (J_{P-C} = 196 Hz); C_{12}: 130.83 (J_{P-C} = 9.3 Hz); C_{13}: 128.37; C_{14}: 132.40. Combustion elemental analysis calculated for $C_{18}H_{18}NO_4P$ (343.10): C, 62.97; H, 5.28; N, 4.08. Found C, 63.07; H, 5.36; N, 4.18%.

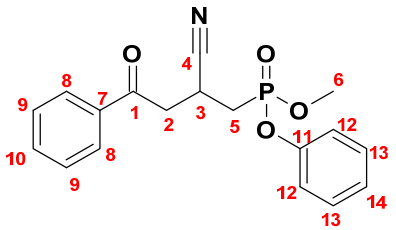

Figure 3. The structure of compound **5c**.

Dimethyl (4-(4-chlorophenyl)-2-cyano-4-oxobutyl)phosphonate **5d** (Figure 4). Yield = 76%; viscous. IR: $\nu_{P=O}$ = 1255 cm^{-1}; $\nu_{C=O}$ = 1675 cm^{-1}; $\nu_{C\,N}$ = 2246 cm^{-1}. ^{31}P-NMR: δ = 31.85,

^{1}H-NMR: (300 MHz, $CDCl_3$) δ: 2.41 ppm (2H, md, $^{2}J_{P-H}$ = 20 Hz, -CH_2-P); 3.21 ppm (2H, m, -CH_2-C=O); 3.72 ppm (6H, d, $^{3}J_{P-H}$ = 10.3 Hz, -O-CH_3); 3.75 ppm (1H, m, >CH-); 7.50 ppm (2H, d,$^{3}J_{HH}$ = 4.5 Hz, ArH); 7.90 (2H, d, $^{3}J_{H-H}$ = 4.5 Hz, ArH). ^{13}C-NMR (300 MHz, $CDCl_3$) δ: C_1: 197.8; C_2: 39.7 (J_{P-C} = 9.5 Hz); C_3: 28.8 (J_{P-C} = 10.1 Hz); C_4: 121.3 (J_{P-C} = 5.2 Hz); C_5: 29.1 (J_{P-C} = 132 Hz); C_6: 53.0 (J_{P-C} = 6.3 Hz); C_7: 134.0; C_8: 129.7 4; C_9: 128.95; C_{10}: 138.18. Combustion elemental analysis calculated for $C_{13}H_{15}ClNO_4P$ (315.04): C, 49.46; H, 4.79; N, 4.44. Found C, 49.58; H, 4.91; N, 4.56%.

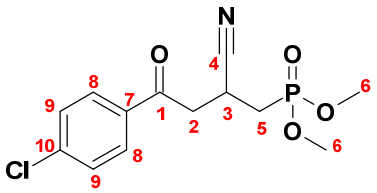

Figure 4. The structure of compound **5d**.

Diethyl (4-(4-chlorophenyl)-2-cyano-4-oxobutyl)phosphonate **5e** (Figure 5). Yield = 73%; viscous. IR: $\nu_{P=O}$ = 1259 cm^{-1}; $\nu_{C=O}$ = 1682 cm^{-1}; ν_{CN} = 2248 cm^{-1}. ^{31}P-NMR: δ = 30.23. ^{1}H-NMR: δ: 1.35 ppm (6H, t, $^{3}J_{H-H}$ = 7.5 Hz, -CH_3); 2.38 ppm (2H, md, $^{2}J_{P-H}$ = 21 Hz, -CH_2-P); 3.25 ppm (2H, m, -CH_2-C=O); 3.79 ppm (1H, m, >CH-); 4.12 ppm (4H, m, -CH_2-O); 7.48 ppm (2H, d, $^{3}J_{H-H}$ = 4.5 Hz, ArH); 7.90 ppm (2H, d, $^{3}J_{H-H}$ = 4.5 Hz, ArH). ^{13}C-NMR (300 MHz, $CDCl_3$) δ: C_1: 197.9; C_2: 40.1 (J_{P-C} = 9.2 Hz); C_3: 29.4 (J_{P-C} = 10.2 Hz); C_4: 122.0 (J_{P-C} = 5.1 Hz); C_5: 28.6 (J_{P-C} = 133 Hz); C_6: 61.8 (J_{P-C} = 7.2 Hz); C_7: 134.5; C_8: 128.81; C_9: 128.91; C_{10}: 139.16; C_{11}: 16.32. Combustion elemental analysis calculated for $C_{15}H_{19}ClNO_4P$ (343.07): C, 52.41; H, 5.57; N, 4.07. Found C, 52.49; H, 5.67; N, 4.20%.

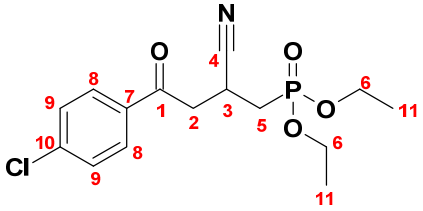

Figure 5. The structure of compound **5e**.

Methyl phenyl (4-(4-chlorophenyl)-2-cyano-4-oxobutyl)phosphonate **5f** (Figure 6). Yield = 68%; viscous. IR: $\nu_{P=O}$ = 1264 cm^{-1}; $\nu_{C=O}$ = 1687 cm^{-1}; ν_{CN} = 2252 cm^{-1}. ^{31}P-NMR: δ = 39.94 ppm.^{1}H-NMR: δ: 2.70 ppm (1H, m, -CH_2-P); 3.02 ppm (1H, m, -CH_2-P); 3.20 ppm (2H, m, -CH_2-C=O); 3.68 ppm (3H, d, $^{3}J_{P-H}$ = 9.5 Hz, CH_3-O); 3.76 ppm (1H, m, >CH-); 7.45–7.72 ppm (9H, m, ArH). ^{13}C-NMR (300 MHz, $CDCl_3$) δ: C_1: 197.6; C_2: 39.6 (J_{P-C} = 8.6 Hz); C_3: 29.1 (J_{P-C} = 8.5 Hz); C_4: 120.6 (J_{P-C} = 4.5 Hz); C_5: 29.4 (J_{P-C} = 98.6 Hz); C_6: 54.1 (J_{P-C} = 6.5 Hz); C_7: 133.6; C_8: 129.88; C_9: 128.94; C_{10}: 138.90; C_{11}: 132.10 (J_{P-C} = 198 Hz); C_{12}: 130.81 (J_{P-C} = 8.3 Hz); C_{13}: 128.22; C_{14}: 132.30. Combustion elemental analysis calculated for $C_{18}H_{17}ClNO_4P$ (377.06): C, 57.23; H, 4.54; N, 3.71. Found C, 57.35; H, 4.63; N, 3.81%.

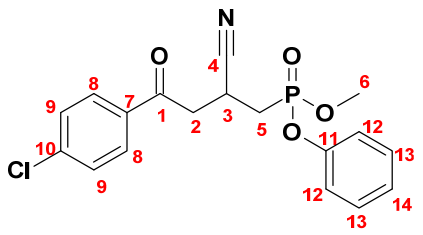

Figure 6. The structure of compound **5f**.

Dimethyl (2-cyano-4-oxo-4-(pyridin-4-yl)butyl)phosphonate **5g** (Figure 7). Yield = 85%; viscous. IR: $\nu_{P=O}$ = 1250 cm^{-1}; $\nu_{C=O}$ = 1674 cm^{-1}; ν_{CN} = 2246 cm^{-1}. ^{31}P-NMR: δ = 31.87.

^{1}H-NMR: (300 MHz, $CDCl_3$) δ: 2.44 ppm (2H, md, $^{2}J_{P\text{-}H}$ = 18,6 Hz, -CH_2-P); 3.32 ppm (2H, m, -CH_2-C=O); 3.65 ppm (6H, d, $^{3}J_{P\text{-}H}$ = 12 Hz, -O-CH_3); 3.79 ppm (1H, m, >CH-); 7.73 ppm (2H, d, $^{3}J_{H\text{-}H}$ = 4.5 Hz, ArH); 8.77 ppm (2H, d, $^{3}J_{H\text{-}H}$ = 4.5 Hz, ArH). ^{13}C-NMR (300 MHz, $CDCl_3$) δ: C_1: 198.2; C_2: 39.8 ($J_{P\text{-}C}$ = 9.4 Hz); C_3: 28.9 ($J_{P\text{-}C}$ = 10.0 Hz); C_4: 121.3 ($J_{P\text{-}C}$ = 5.0 Hz); C_5: 29.1 ($J_{P\text{-}C}$ = 135 Hz); C_6: 53.1 ($J_{P\text{-}C}$ = 6.2 Hz); C_7: 139.8; C_8: 121.21; C_9: 149.50. Combustion elemental analysis calculated for $C_{12}H_{15}N_2O_4P$ (282.08): C, 51.07; H, 5.36; N, 9.93. Found C, 51.16; H, 5.44; N, 9.84%.

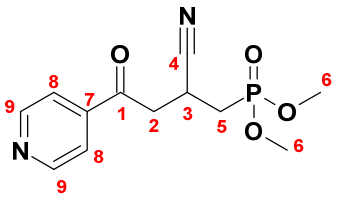

Figure 7. The structure of compound **5g**.

Diethyl (2-cyano-4-oxo-4-(pyridin-4-yl)butyl)phosphonate **5h** (Figure 8). Yield = 84%; viscous. IR: $\nu_{P=O}$ = 1247 cm^{-1}; $\nu_{C=O}$ = 1680 cm^{-1}; ν_{CN} = 2250 cm^{-1}. ^{31}P-NMR: δ = 30.79. ^{1}H-NMR: δ: 1.35 ppm (6H, t, $^{3}J_{H\text{-}H}$ = 7.4 Hz, -CH_3); 2.36 ppm (2H, md, $^{2}J_{P\text{-}H}$ = 23 Hz, -CH_2-P); 3.27 ppm (2H, m, -CH_2-C=O); 3.82 ppm (1H, m, >CH-); 4.11 ppm (4H, qd, $^{3}J_{H\text{-}H}$ = 7.4 Hz, $^{3}J_{P\text{-}H}$ = 9.6 Hz, -CH_2-O); 7.76 ppm (2H, d, $^{3}J_{H\text{-}H}$ = 3.5 Hz, ArH); 8.78 ppm (2H, d, $^{3}J_{H\text{-}H}$ = 3.5 Hz, ArH). ^{13}C-NMR (300 MHz, $CDCl_3$) δ: C_1: 198.3; C_2: 40.5 ($J_{P\text{-}C}$ = 9.6 Hz); C_3: 29.1 ($J_{P\text{-}C}$ = 10.1 Hz); C_4: 121.9 ($J_{P\text{-}C}$ = 5.1 Hz); C_5: 28.6 ($J_{P\text{-}C}$ = 138 Hz); C_6: 61.9 ($J_{P\text{-}C}$ = 6.4 Hz); C_7: 140.0; C_8: 121.15; C_9: 149.36; C_{10}: 16.35. Combustion elemental analysis calculated for $C_{14}H_{19}N_2O_4P$ (310.11): C, 54.19; H, 6.17; N, 9.03. Found C, 54.28; H, 6.25; N, 9.13%.

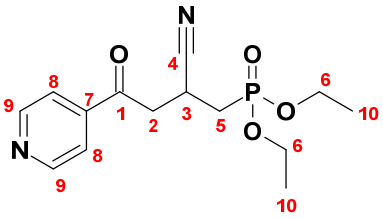

Figure 8. The structure of compound **5h**.

Methyl phenyl (2-cyano-4-oxo-4-(pyridin-4-yl)butyl)phosphonate **5i** (Figure 9). Yield = 82%; viscous. IR: $\nu_{P=O}$ = 1258 cm^{-1}; $\nu_{C=O}$ = 1688 cm^{-1}; ν_{CN} = 2251 cm^{-1}. ^{31}P-NMR: δ = 40.96. ^{1}H-NMR: δ: 2.69 ppm (1H, m, -CH_2-P); 3.01 ppm (1H, m, -CH_2-P); 3.31 ppm (2H, m, -CH_2-C=O); 3.70 ppm (3H, d,$^{3}J_{P\text{-}H}$ = 9.3 Hz, CH_3-O); 3.80 ppm (1H, m, >CH-); 7.46–7.74 ppm (5H, m, Ph); 7.50 ppm (2H, m, ArH); 7.76 ppm (2H, m, ArH). ^{13}C-NMR (300 MHz, $CDCl_3$) δ: C_1: 197.8; C_2: 37.9 ($J_{P\text{-}C}$ = 7.9 Hz); C_3: 29.3 ($J_{P\text{-}C}$ = 9.2 Hz); C_4: 122.2 ($J_{P\text{-}C}$ = 4.6 Hz); C_5: 30.3 ($J_{P\text{-}C}$ = 105 Hz); C_6: 53.4 ($J_{P\text{-}C}$ = 6.2 Hz); C_7: 140.0; C_8: 120.82; C_9: 149.32; C_{10}: 132.11($J_{P\text{-}C}$ = 198 Hz); C_{11}: 130.59 ($J_{P\text{-}C}$ = 8.7 Hz); C_{12}: 128.07; C_{13}: 132.43. Combustion elemental analysis calculated for $C_{17}H_{17}N_2O_4P$ (344.09): C, 59.30; H, 4.98; N, 8.14. Found C, 59.38; H, 4.88; N, 8.23%.

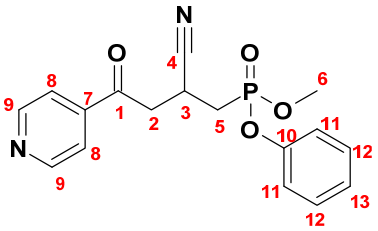

Figure 9. The structure of compound **5i**.

Dimethyl (2-cyano-4-(4-methoxyphenyl)-4-oxobutyl)phosphonate **5j** (Figure 10). Yield = 77%; viscous. IR: $\nu_{P=O}$ = 1259 cm^{-1}; $\nu_{C=O}$ = 1682 cm^{-1}; ν_{CN} = 2243 cm^{-1}. ^{31}P-NMR: δ = 31.76 ppm. ^{1}H-NMR: (300 MHz, $CDCl_3$) δ: 2.44 ppm (2H, md, $^{2}J_{P-H}$ = 18.5 Hz, -CH_2-P); 3.22 ppm (2H, d,$^{3}J_{H-H}$ = 8.3 Hz -CH_2-C=O); 3.74 ppm (6H, d,$^{3}J_{P-H}$ = 9.5 Hz, -O-CH_3); 3.77 ppm (1H, m, >CH-); 3.85 ppm (3H, s, CH_3-O-);7.00 ppm (2H, d, $^{3}J_{HH}$ = 4.2 Hz, ArH); 7.96 (2H, d, $^{3}J_{H-H}$ = 4.2 Hz, ArH). ^{13}C-NMR (300 MHz, $CDCl_3$) δ: C_1: 198.2; C_2: 40.5 (J_{P-C} = 9.2 Hz); C_3: 28.9 (J_{P-C} = 10.3 Hz); C_4: 121.9 (J_{P-C} = 5.1 Hz); C_5: 29.2 (J_{P-C} = 132 Hz); C_6: 52.8 (J_{P-C} = 6.3 Hz); C_7: 131.3; C_8: 129.94; C_9: 117.61; C_{10}: 163.29; C_{11}: 55.34. Combustion elemental analysis calculated for $C_{14}H_{18}NO_5P$ (311.09): C, 54.02; H, 5.83; N, 4.50. Found C, 54.14; H, 5.93; N, 4.58%.

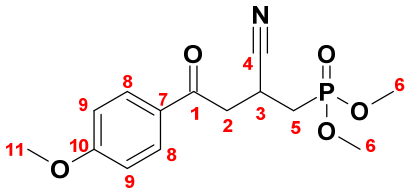

Figure 10. The structure of compound **5j**.

Diethyl (2-cyano-4-(4-methoxyphenyl)-4-oxobutyl)phosphonate **5k** (Figure 11). Yield = 74%; viscous. IR: $\nu_{P=O}$ = 1263 cm^{-1}; $\nu_{C=O}$ = 1678 cm^{-1}; ν_{CN} = 2251 cm^{-1}. ^{31}P-NMR: δ = 30,31 ppm. ^{1}H-NMR: δ: 1.34 ppm (6H, q, $^{3}J_{H-H}$ = 7.5 Hz, -CH_3); 2.38 ppm (2H, md, $^{2}J_{P-H}$ = 21.0 Hz, -CH_2-P); 3.17 ppm (2H, d, $^{3}J_{H-H}$ = 7.5 Hz, -CH_2-C=O); 3.79 ppm (1H, m, >CH-); 3.84 ppm (3H, s, CH_3-O); 4.07 ppm (4H, m, -CH_2-O); 6.99 ppm (2H, d,$^{3}J_{H-H}$ = 4.0 Hz, ArH); 7.92 ppm (2H, d, $^{3}J_{H-H}$ = 4.0 Hz, ArH). ^{13}C-NMR (300 MHz, $CDCl_3$) δ: C_1: 198.4; C_2: 40.2 (J_{P-C} = 9.4 Hz); C_3: 29.2 (J_{P-C} = 10.1 Hz); C_4: 122.0 (J_{P-C} = 5.3 Hz); C_5: 28.7 (J_{P-C} = 133 Hz); C_6: 60.7 (J_{P-C} = 6.4 Hz); C_7: 131.6; C_8: 130.00; C_9: 117.73; C_{10}: 163.12; C_{11}: 55.07. Combustion elemental analysis calculated for $C_{16}H_{22}NO_5P$ (339.12): C, 56.63; H, 6.53; N, 4.13. Found C, 56.75; H, 6.64; N, 4.22%.

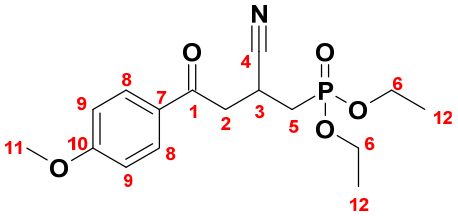

Figure 11. The structure of compound **5k**.

Methyl phenyl (2-cyano-4-(4-methoxyphenyl)-4-oxobutyl)phosphonate **5l** (Figure 12). Yield = 71%; viscous. IR: $\nu_{P=O}$ = 1247 cm^{-1}; $\nu_{C=O}$ = 1682 cm^{-1}; ν_{CN} = 2247 cm^{-1}. ^{31}P-NMR: δ = 41.52. ^{1}H-NMR: δ: 2.85 ppm (1H, dd, $^{3}J_{H-H}$ = 6.8 Hz, $^{2}J_{P-H}$ = 18 Hz, -CH_2-P); 2.85 ppm (1H, dd, $^{3}J_{H-H}$ = 6.8 Hz, $^{2}J_{P-H}$ = 18 Hz, -CH_2-P); 3.17 ppm (2H, dd, $^{4}J_{P-H}$ = 3.1 Hz, $^{3}J_{H-H}$ = 7.2 Hz, -CH_2-C=O); 3.70 ppm (3H, d, $^{3}J_{P-H}$ = 9.2 Hz, CH_3-O); 3.75 ppm (1H, m, >CH-); 3.82 ppm (3H, s, CH_3-O); 7.00 ppm (2H, d, $^{3}J_{H-H}$ = 4.2 Hz, ArH); 7.96 ppm (2H, d, $^{3}J_{H-H}$ = 4.2 Hz, ArH); 7.50–7.75 ppm (5H, m, Ph); ^{13}C-NMR (300 MHz, $CDCl_3$) δ: C_1: 198.1; C_2: 40.3 (J_{P-C} = 8.7 Hz); C_3: 29.1 (J_{P-C} = 8.3 Hz); C_4: 120.8 (J_{P-C} = 4.8 Hz); C_5: 30.5 (J_{P-C} = 97.7 Hz); C_6: 53.4 (J_{P-C} = 6.2 Hz); C_7: 131.5; C_8: 130.00; C_9: 117.20; C_{10}: 163.21; C_{11}: 55.53; C_{12}: 132.10 (J_{P-C} = 196 Hz); C_{13}: 130.80 (J_{P-C} = 8.8 Hz); C_{14}: 128.19. Combustion elemental analysis calculated for $C_{19}H_{20}NO_5P$ (373.11): C, 61.12; H, 5.40; N, 3.75. Found C, 61.23; H, 5.49; N, 3.83%.

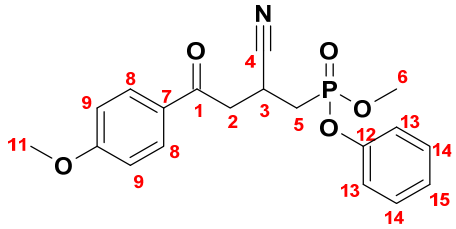

Figure 12. The structure of compound **5l**.

5. Molecular Docking Study

5.1. Protein and Ligand Preparation

The progesterone receptor protein structure was received in PDB format from RCSB PDB (ID: 1E3K) and the structure of 3CLpro from SARS-CoV19 (ID: 1UK4), and they were prepared using Discovery Studio 2019 to remove ligands and water molecules [27]. ChemDraw3D Ultra provided the SDF format for the ligand structures.

Molecular Docking

Polar hydrogens and Kollman charges were applied to the protein, and a pdbqt format file was generated using the AutoDockTools 1.5.6 program. The protein was created using the protein preparation wizard in AutoDockTools 1.5.6. Polar hydrogens and Kollman charges were applied to the protein, and a pdbqt format file was generated using AutoDockTools. Both 1UK4 and 1E3K were completely devoid of water molecules. The ligand torsions were calculated by first detecting the roots in AutoDockTools 1.5.6, and then setting the aromaticity parameters to 7.5. The receptor was given a grid size of 60 Å × 60 Å × 60 Å, and the molecular docking operation was assigned to the Lamarckian genetic algorithm (LGA). After docking, the best pose was chosen based on binding energy, ligand–receptor interactions, and active site residues. The docked posture was simply compared to the cocrystallized structure, and the root mean square deviation (RMSD) was less than 1.0 Å. All torsions were allowed to rotate during docking. The traditional docking procedure for rigid and fluid ligand docking included 10 separate runs per ligand, 2.5×10^6 energy measurements, a total of 27,000 iterations, a mutation rate of 0.02, a crossover rate of 0.80, and an elitism value of 1. The likelihood of conducting a local search on a person in the population was 0.06 using a limit of 300 iterations per local search. Following docking, the 10 solutions were classified as having RMS differences of less than 1.0. The clusters were sorted based on the cluster's lowest energy representation. The effects of the docking process were visualized using the BIOVIA Discovery Studio program.

6. Conclusions

A molecular docking study was used to determine the binding energy for nonbonding interactions between the ligand (synthesized compounds) and receptors (1UK4 and 1E3K). All the compounds studied formed stable complexes with receptors that had a high binding energy. Compound **5i** had the best docking energy (highest binding energy) according to our findings, with a binding affinity of (−8.65 kcal/mol with 1UK4, and −10.41 kcal/mol with 1E3K), as in Table 1.

Supplementary Materials: The following supporting information can be downloaded, Mol file of 4-Aryl-2-dialkylphosphonomethyl-4-oxobutanenitrile; Figure S1: molecular docked model of compounds **3a**–**5a** with (1uk4): (the target is presented as thin sticks; the ligands are drawn as ball-and-stick) where (a–d) represent the 3D docking styles for 1uk4 with compounds **3a**, **3b**, **3e** and **5a**, respectively, and (e–h) represent the 2D docking styles for 1uk4 with compounds **3a**, **3b**, **3e** and **5a**, respectively; Figure S2: molecular docked model of compounds **5b**–**5e** with (1uk4): (the target is presented as thin sticks; the ligands are drawn as ball-and-stick) where (i–l) represent the 3D docking styles for 1uk4 with compounds **5b**, **5c**, **5d** and **5e**, respectively, and (m–p) represent the 2D docking styles for 1uk4 with compounds **5b**, **5c**, **5d** and **5e**, respectively; Figure S3: molecular docked model of compounds **5f**–**5i** with (1uk4): (the target is presented as thin sticks; the ligands are

drawn as ball-and-stick) where (q–t) represent the 3D docking styles for 1uk4 with compounds **5f**, **5g**, **5h** and **5i**, respectively, and (u–x) represent the 2D docking styles for 1uk4 with compounds **5f**, **5g**, **5h** and 5i, respectively; Figure S4: molecular docked model of compounds **5j** and **5k** with (1uk4): (the target is presented as thin sticks; the ligands are drawn as ball-and-stick) where (y,z) represent the 3D docking styles for 1uk4 with compounds **5j** and **5k**, respectively, and (A,B) represent the 2D docking styles for 1uk4 with compounds **5j** and **5k**, respectively; Figure S5: molecular docked model of compounds **3a**–**3e** with (1e3k): (the target is presented as thin sticks; the ligands are drawn as ball-and-stick) where (A–C) represent the 3D docking styles for 1e3k with compounds **3a**, **3b** and **3e**, respectively, and (D–F) represent the 2D docking styles for 1e3k with compounds **3a**, **3b** and **3e**, respectively; Figure S6: molecular docked model of compounds **5a**–**5c** with (1e3k): (the target is presented as thin sticks; the ligands are drawn as ball-and-stick) where (G–I) represent the 3D docking styles for 1e3k with compounds **5a**, **5b** and **5c**, respectively, and (J–L) represent the 2D docking styles for 1e3k with compounds **5a**, **5b** and **5c**, respectively; Figure S7: molecular docked model of compounds **5d**–**5g** with (1e3k): (the target is presented as thin sticks; the ligands are drawn as ball-and-stick) where (M–P) represent the 3D docking styles for 1e3k with compounds **5d**, **5e**, **5f** and **5g**, respectively, and (Q–T) represent the 2D docking styles for 1e3k with compounds **5d**, **5e**, **5f** and **5g**, respectively; Figure S8: molecular docked model of compounds **5h**–**5k** with (1e3k): (the target is presented as thin sticks; the ligands are drawn as ball-and-stick) where (U–X) represent the 3D docking styles for 1e3k with compounds **5h**, **5i**, **5j** and **5k**, respectively, and (Y,Z,a,b) represent the 2D docking styles for 1e3k with compounds **5h**, **5i**, **5j** and **5k**, respectively. Figure S9: ^{1}H-NMR spectra of diethyl (2-cyano-4-oxo-4-phenylbutyl)phosphonate **5b**. Figure S10: ^{13}C-NMR spectra of diethyl (2-cyano-4-oxo-4-phenylbutyl)phosphonate **5b**. Figure S11: 31P-NMR spectra of diethyl (2-cyano-4-oxo-4-phenylbutyl)phosphonate **5b**. Figure S12: ^{1}H-NMR spectra of dimethyl (4-(4-chlorophenyl)-2-cyano-4-oxobutyl)phosphonate **5d**. Figure S13: ^{13}C-NMR spectra of dimethyl (4-(4-chlorophenyl)-2-cyano-4-oxobutyl)phosphonate **5d**. Figure S14: ^{31}P-NMR spec-tra of dimethyl (4-(4-chlorophenyl)-2-cyano-4-oxobutyl)phosphonate **5d**. Figure S15: ^{1}H-NMR spectra of methyl phenyl (4-(4-chlorophenyl)-2-cyano-4-oxobutyl)phosphonate **5f**. Figure S16: ^{13}C-NMR spectra of methyl phenyl (4-(4-chlorophenyl)-2-cyano-4-oxobutyl)phosphonate **5f**. Figure S17: ^{31}P-NMR spectra of methyl phenyl (4-(4-chlorophenyl)-2-cyano-4-oxobutyl)phosphonate **5f**. Figure S18: ^{1}H-NMR spectra of dime-thyl (2-cyano-4-oxo-4-(pyridin-4-yl)butyl)phosphonate **5g**. Figure S19: ^{13}C-NMR spectra of di-methyl (2-cyano-4-oxo-4-(pyridin-4-yl)butyl)phosphonate **5g**. Figure S20: ^{31}P-NMR spectra of dimethyl (2-cyano-4-oxo-4-(pyridin-4-yl)butyl)phosphonate **5g**. Figure S21: ^{1}H-NMR spectra of diethyl (2-cyano-4-oxo-4-(pyridin-4-yl)butyl)phosphonate **5h**. Figure S22: ^{13}C-NMR spectra of di-ethyl (2-cyano-4-oxo-4-(pyridin-4-yl)butyl)phosphonate **5h**. Figure S23: ^{31}P-NMR spectra of di-ethyl (2-cyano-4-oxo-4-(pyridin-4-yl)butyl)phosphonate **5h**. Figure S24: ^{1}H-NMR spectra of me-thyl phenyl (2-cyano-4-(4-methoxyphenyl)-4-oxobutyl)phosphonate **5l**. Figure S25: ^{13}C-NMR spectra of methyl phenyl (2-cyano-4-(4-methoxyphenyl)-4-oxobutyl)phosphonate **5l**. Figure S26: ^{31}P-NMR spectra of methyl phenyl (2-cyano-4-(4-methoxyphenyl)-4-oxobutyl)phosphonate **5l**.

Author Contributions: F.Y., H.E., H.S.M., Z.S.H. and Y.H.Z. designed the research, performed the research, analyzed the data, wrote the paper, and approved the final manuscript. All authors have read and agreed to the published version of the manuscript.

Funding: This research received no external funding.

Institutional Review Board Statement: Not applicable.

Informed Consent Statement: Not applicable.

Data Availability Statement: The data presented in this study are available on request from the corresponding author.

Conflicts of Interest: The authors declare no conflict of interest.

Sample Availability: Samples of the compounds are available from the authors.

References

1. Iida, H.; Moromizato, T.; Hamana, H.; Matsumoto, K. An efficient conjugate hydrocyanation of chalcones and related enones with TMSCN under solvent-and additive-free microwave conditions. *Tetrahedron Lett.* **2007**, *48*, 2037–2039. [CrossRef]
2. Stetter, H.; Schreckenberg, M. Addition of aldehydes to activated double bonds. *Angew. Chem.* **1973**, *85*, 89. [CrossRef]

3. Stetter, H. Addition aliphatischer Aldehyde an aktivierte Doppelbindungen. *Angew. Chem.* **1974**, *86*, 589. [CrossRef]
4. Kaminski, T. Synthèse de dérivés de la 4-(méthylnitroasamino)-1-(3-pyridyl)-1-butanone (NNK). Ph.D. Thesis, Université Paul Verlaine-Metz, Metz, France, 2007.
5. Stetter, H.; Kuhlmann, H. Addition von aliphatischen, heterocyclischen und aromatischen Aldehyden an α, β-ungesättigte Ketone, Nitrile und Ester. *Chem. Ber.* **1976**, *109*, 2890–2896. [CrossRef]
6. Mrabet, H.; Zantour, H. Nouvelles voies d'acces aux 2-ethoxycarbonylallylphosphonates. *Phosphorus Sulfur Silicon* **2004**, *179*, 25–33. [CrossRef]
7. Yaccoubi, F.; Efrit, M.; Zantour, H. Synthèse d'aminopyrazolines phosphonométhylées. *J. Soc. Chim. Tunis.* **2005**, *7*, 89–96.
8. Abdelli, A.; Efrit, M.L.; Gaucher, A.; M'rabet, H.; Prim, D. A convenient synthesis of phosphonomethyl α, β-unsaturated γ-lactams. *Tetrahedron Lett.* **2015**, *56*, 5397–5400. [CrossRef]
9. Abdelli, A.; M'rabet, H.; Efrit, M.L.; Gaucher, A.; Prim, D. γ-Alkylsulfide phosphonates through the thia-Michael strategy. *J. Sulfur Chem.* **2014**, *35*, 674–682. [CrossRef]
10. Grushin, V.V. Generation of "Naked" Fluoride Ions in Unprecedentedly High Concentrations from a Fluoropalladium Complex. *Angew. Chem. Int. Ed.* **1998**, *37*, 994–996. [CrossRef]
11. Dong, E.; Du, H.; Gardner, L. An interactive web-based dashboard to track COVID-19 in real time. *Lancet Infect. Dis.* **2020**, *20*, 533–534. [CrossRef]
12. Macchiagodena, M.; Pagliai, M.; Procacci, P. Identification of potential binders of the main protease 3CLpro of the COVID-19 via structure-based ligand design and molecular modeling. *Chem. Phys. Lett.* **2020**, *750*, 137489. [CrossRef]
13. Sayers, E.W.; Beck, J.; Bolton, E.E.; Bourexis, D.; Brister, J.R.; Canese, K.; Comeau, D.C.; Funk, K.; Kim, S.; Klimke, W. Database resources of the national center for biotechnology information. *Nucleic Acids Res.* **2021**, *49*, D10. [CrossRef] [PubMed]
14. Shanker, A.; Bhanu, D.; Alluri, A. Analysis of Whole Genome Sequences and Homology Modelling of a 3-C Like Peptidase and a Non-Structural Protein of the Novel Coronavirus COVID-19 Shows Protein Ligand Interaction with an Aza-Peptide and a Noncovalent Lead Inhibitor with Possible Antiviral Properties. *ChemRxiv* **2020**. [CrossRef]
15. Thiel, V.; Ivanov, K.A.; Putics, A.; Hertzig, T.; Schelle, B.; Bayer, S.; Weißbrich, B.; Snijder, E.J.; Rabenau, H.; Doerr, H.W. Mechanisms and enzymes involved in SARS coronavirus genome expression. *J. Gen. Virol.* **2003**, *84*, 2305–2315. [CrossRef] [PubMed]
16. Hilgenfeld, R. From SARS to MERS: Crystallographic studies on coronaviral proteases enable antiviral drug design. *FEBS J.* **2014**, *281*, 4085–4096. [CrossRef] [PubMed]
17. Fouad, S.A.; El-Gendey, M.S.; Ahmed, E.M.; Hessein, S.A.; Ammar, Y.A.; Zaki, Y.H. Convenient Synthesis of Some New Thiophene, Pyrazole, and Thiazole Derivatives Bearing Biologically Active Sulfonyl Guanidine Moiety. *Polycycl. Aromat. Compd.* **2021**, 1–19. [CrossRef]
18. Nassan, M.A.; Aldhahrani, A.; Amer, H.H.; Elhenawy, A.; Swelum, A.A.; Ali, O.M.; Zaki, Y.H. Investigation of the Anticancer Effect of α-Aminophosphonates and Arylidine Derivatives of 3-Acetyl-1-aminoquinolin-2(1H)-one on the DMBA Model of Breast Cancer in Albino Rats with In Silico Prediction of Their Thymidylate Synthase Inhibitory Effect. *Molecules* **2022**, *27*, 756. [CrossRef]
19. Hosny, M.A.; Zaki, Y.H.; Mokbel, W.A.; Abdelhamid, A.O. Synthesis, characterization, antimicrobial activity and anticancer of some new pyrazolo [1, 5-a] pyrimidines and pyrazolo [5, 1-c] 1, 2, 4-triazines. *Med. Chem.* **2020**, *16*, 750–760. [CrossRef]
20. Gomha, S.M.; Zaki, Y.H.; Abdelhamid, A.O. Utility of 3-Acetyl-6-bromo-2H-chromen-2-one for the synthesis of new heterocycles as potential antiproliferative agents. *Molecules* **2015**, *20*, 21826–21839. [CrossRef]
21. Zaki, Y.H.; Gomha, S.M.; Mohamed, A.M.G. Utility of 2-thioxo-pyrido [2, 3-d] pyrimidinone in synthesis of pyridopyrimido [2, 1-b] [1, 3, 5]-thiadiazinones and pyridopyrimido [2, 1-b] [1, 3] thiazinones as antimicrobial agents. *Chem. Cent. J.* **2017**, *11*, 57. [CrossRef]
22. Yang, H.; Yang, M.; Ding, Y.; Liu, Y.; Lou, Z.; Zhou, Z.; Sun, L.; Mo, L.; Ye, S.; Pang, H. The crystal structures of severe acute respiratory syndrome virus main protease and its complex with an inhibitor. *Proc. Natl. Acad. Sci. USA* **2003**, *100*, 13190–13195. [CrossRef]
23. Brilliana, D. Faktor Yang Berhubungan Dengan Perilaku Ibu Rumah Tangga Melakukan Pemeriksaan Payudara Sendiri (Sadari). *Indones J. Public Health* **2017**, *12*, 143–153.
24. Sulung, N.; Yananda, R.; Suwito, A. Determinan Kejadian Ca Mammae Di Poli Rawat Jalan Bedah Rsud Dr. Achmad Mochtar. *J. Endur. Kaji. Ilm. Probl. Kesehat.* **2018**, *3*, 575–587. [CrossRef]
25. Zhang, X.; Shen, T.; Zhou, X.; Tang, X.; Gao, R.; Xu, L.; Wang, L.; Zhou, Z.; Lin, J.; Hu, Y. Network pharmacology based virtual screening of active constituents of *Prunella vulgaris* L. and the molecular mechanism against breast cancer. *Sci. Rep.* **2020**, *10*, 15730. [CrossRef]
26. Hoffmann, J.; Lichtner, R.B.; Fuhrmann, U.; Hess-Stumpp, H.; Siemeister, G.; Cleve, A.; Neef, G.; Parczyk, K.; Schneider, M.R. New progesterone receptor antagonists preventing carcinogen induced breast cancer in rats. *Proc. Amer. Assoc. Cancer Res.* **2004**, *45*.
27. Biovia, D. *Discovery Studio Visualizer*; Dassault Systèmes: San Diego, CA, USA, 2017.